

Article

Hydrologic Evaluation of Six High Resolution Satellite Precipitation Products in Capturing Extreme Precipitation and Streamflow over a Medium-Sized Basin in China

Shanhu Jiang ^{1,2}, Shuya Liu ^{1,2}, Liliang Ren ^{1,2,*}, Bin Yong ¹, Linqi Zhang ², Menghao Wang ², Yujie Lu ² and Yingqing He ³

¹ State Key Laboratory of Hydrology-Water Resources and Hydraulic Engineering, Hohai University, Nanjing 210098, China; hik0216@hhu.edu.cn (S.J.); vavavavi@hhu.edu.cn (S.L.); yongbin_hhu@126.com (B.Y.)

² College of Hydrology and Water Resources, Hohai University, Nanjing 210098, China; zhanglinqi008@163.com (L.Z.); 13253671875@163.com (M.W.); luyujiefighting@163.com (Y.L.)

³ Nanjing Branch, Huai'an Surveying and Design Institute of Water Resources Co., Ltd., Nanjing 210008, China; butterfly198474@sina.com

* Correspondence: njRLL9999@126.com; Tel.: +86-25-8378-7480

Received: 22 November 2017; Accepted: 25 December 2017; Published: 29 December 2017

Abstract: Satellite precipitation products (SPPs) are critical data sources for hydrological prediction and extreme event monitoring, especially for ungauged basins. This study conducted a comprehensive hydrological evaluation of six mainstream SPPs (i.e., TMPA 3B42RT, CMORPH-RT, PERSIANN-RT, TMPA 3B42V7, CMORPH-CRT, and PERSIANN-CDR) over humid Xixian basin in central eastern China for a period of 14 years (2000–2013). The evaluation specifically focused on the performance of the six SPPs in capturing precipitation and streamflow extremes. Results show that the two post-real-time research products of TMPA 3B42V7 and CMORPH-CRT exhibit much better performance than that of their corresponding real-time SPPs for precipitation estimation at daily and monthly time scales. By contrast, the newly released post-real-time research product PERSIANN-CDR insignificantly improves precipitation estimates compared with the real-time PERSIANN-RT does at daily time scale. The daily streamflow simulation of TMPA 3B42V7 fits best with the observed streamflow series among those of the six SPPs. The three month-to-month gauge-adjusted post-real-time research products can simulate acceptable monthly runoff series. TMPA 3B42V7 and CMORPH-CRT present good performance in capturing precipitation and streamflow extremes, although they still exhibit non-ignorable deviation and occurrence time inconsistency problems compared with gauge-based results. Caution should be observed when using the current TMPA, CMORPH, and PERSIANN products for monitoring and predicting extreme precipitation and flood at such medium-sized basin. This work will be valuable for the utilization of SPPs in extreme precipitation monitoring, streamflow forecasting, and water resource management in other regions with similar climate and topography characteristics.

Keywords: satellite precipitation product; streamflow simulation; extreme precipitation; extreme streamflow; statistical evaluation

1. Introduction

Extreme precipitation and flood often exert serious impacts on human society and infrastructure [1]. According to Global Assessment Report on Disaster Risk Reduction, floods affect people worldwide more than any other natural hazards, with an estimated global annual average loss

of \$104 billion [2]. Accurate precipitation estimates and reliable flood modeling are critical to numbers of national and regional agencies for disaster monitoring, mitigation, and management [3–6]. In recent decades, satellite precipitation products (SPPs) have become new alternative precipitation datasets for global hydrometeorological research and applications [7–9]. For example, the Precipitation Estimation from Remote Sensing Information using Artificial Neural Network (PERSIANN) [10], the Climate Precipitation Center (CPC) Morphing Technique (CMORPH) by National Oceanic and Atmospheric Administration (NOAA) [11], the Tropical Rainfall Measuring Mission Multi-satellite Precipitation Analysis (TMPA) [12], and the Global Precipitation Measurement (GPM) [13], have recently been made operationally available. Among such SPPs, TMPA, CMORPH, and PERSIANN play important roles owing to their long-term series datasets and adequate retrieval experiences and techniques. Before and after the GPM mission implemented on 27 February 2014, the TMPA, CMORPH, and PERSIANN systems have been continuously upgrading their retrieval algorithms and releasing their latest satellite precipitation products [14–16].

In recent years, many works have been made to analyze the accuracy and hydrological utility of the latest SPPs over different topographic or climatic regions all over the world, and they found that the errors of different SPPs depend significantly on the precipitation retrieval algorithm, geographical location, topography condition (plain or mountainous), and seasonality [17–24]. For example, Yong et al. [17] compared the precipitation products of TMPA over two different latitude basins with independent gauge observations and concluded that TMPA exhibit much better performance over the low latitude Mishui basin than over the high latitude Laohahe basin. Zhu et al. [18] evaluated the hydrological utility of TRMM 3B42V7, PERSIANN-CDR, and NCEP-CFSR over two Chinese humid watersheds and found that TMPA 3B42V7 and PERSIANN-CDR present good performance for daily and monthly streamflow simulations. Hussain et al. [22] assessed six SPPs (real-time and bias-adjusted TMPA, CMORPH, and PERSIANN) over plain, mountainous, and glacial regions in Pakistan and concluded that TMPA 3B42V7 and CMORPH-CRT show the best agreement with in situ data over the entire study area.

Some efforts have also been made to evaluate the utility of these SPPs in capturing extreme precipitation and streamflow over different spatial scales [25–34]. Huang et al. [26] evaluated the utility of TMPA 3B42RT and 3B42V7 in capturing one typical extreme rainfall event in Beijing on 21 July 2012 and emphasized that both SPPs present large deviations from the temporal variation in rainfall and underestimate the storm. Miao et al. [27] evaluated PERSIANN-CDR in capturing the extreme precipitation over China and found that PERSIANN-CDR underestimates the values of extreme heavy precipitation. Shah and Mishra [29] analyzed uncertainty and bias in five SPPs over Indian sub-continental basins and highlighted that bias in SPPs affects the initial condition and precipitation forcing, thereby affecting flood peak timing and magnitudes. Mei et al. [31] analyzed error in SPPs-driven flood simulations in complex alpine terrain in Italy and found a dampening effect in both systematic and random error components of the satellite-driven hydrograph relative to the satellite-retrieved hydrograph. These previous researches provided important references for application on SPPs in flood hydrology. However, the further researches of uncertainties of these SPPs in capturing extreme precipitation in terms of rainfall amount deviation and occurrence time inconsistency in different regions and their error propagation characteristics in flood simulation are still needed.

This study focuses on comprehensive hydrological evaluation of six long-term series SPPs (i.e., TMPA 3B42RT, CMORPH-RT, PERSIANN-RT, TMPA 3B42V7, CMORPH-CRT, and PERSIANN-CDR) in humid Xixian basin in central eastern China. This study mainly aims to (1) evaluate the accuracy of six mainstream SPPs with rain gauge observations, (2) validate the hydrological simulation utility of the SPPs via hydrological modeling, and (3) analyze the uncertainties of the SPPs in capturing extreme precipitation and extreme streamflow. This work is valuable for the utilization of SPPs in extreme precipitation monitoring, streamflow forecasting, and water resource management in central eastern China and other regions with similar climate and topography characteristics.

2. Study Area and Data

2.1. Study Area

Xixian Basin, the upstream catchment of Huai River, was selected as our case study area (Figure 1). Extended from longitudes 113.25° E to 115° E and latitudes 31.5° N to 32.75° N, the Xixian basin has a drainage area of 10,191 km² above the Xixian hydrologic station. The elevation within the basin ranges from 33 m to 1110 m. The land use and land coverage in Xixian basin is 54.4% forest and shrubs, 33.5% grassland, 11.8% cropland, and 0.3% urban and water. The basin lies in the transition zone of the mid-latitude humid climate and semi-arid climate. The long term mean annual precipitation and temperature are 1145 mm and 15.2 °C, respectively. The seasonal distribution of the precipitation in the basin is mainly affected by monsoon climate and the vast majority of the annual precipitation falls in the summer season. During these months, particularly in June and July, basin-wide heavy rains continuously occur, thereby resulting in floods. The long term mean annual cumulative flow rate is 3.58×10^9 m³ at Xixian hydrologic station.

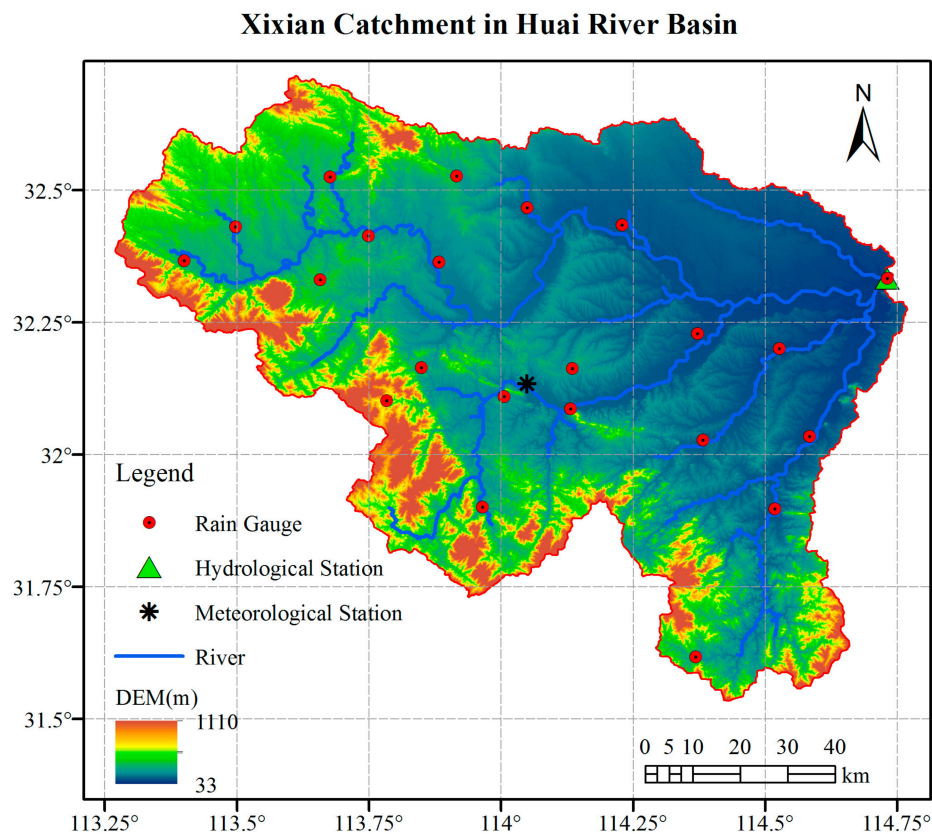


Figure 1. Map of Xixian Basin in upstream of Huai River Basin.

2.2. Data

2.2.1. Satellite Precipitation Products

The SPPs used in this study are three pure real-time SPPs, namely, TMPA 3B42RT, CMORPH-RT, and PERSIAN-RT, and three post-real-time research SPPs, namely, TMPA 3B42V7, CMORPH-CRT, and PERSIANN-CDR.

The TMPA combines the low-orbit satellite microwave (MW) data where available and the MW-calibrated geostationary infrared (IR) data elsewhere to produce quasi-global (50° N-S) precipitation dataset [12]. The TMPA 3B42RT and TMPA 3B42V7 precipitation products were produced

by the latest TMPA Version 7 algorithms upgraded on 28 January 2013 [14]. During the past years, hydrologists and meteorologists have widely evaluated and applied the TMPA products [17,18,20–26]. While, the utility of the latest version 7 TMPA products in capturing extreme precipitation and streamflow has not been fully evaluated at river basin scale.

The CMORPH is primarily based on low-orbit satellite MW observations, and the geostationary IR data are used only to derive the movement of precipitation systems [11]. At NOAA CPC, CMORPH reprocessed a new dataset named CMORPH Version 1.0 in 2014. CMORPH Version 1.0 includes the raw, satellite-only precipitation estimates (CMORPH-RT) and the new bias-corrected precipitation products (CMORPH-CRT). CMORPH-CRT adjusts precipitation estimate through matching the PDF of daily CMORPH-RT against that for the CPC unified daily gauge analysis at each month over land [15].

The PERSIANN derives the relationships between IR and MW data by a neural network approach and then apply the relationships to the IR data to generate real-time precipitation products (PERSIANN-RT) [10]. PERSIANN-CDR is a newly developed bias-adjusted satellite precipitation product that covers from 1 January 1983 to present [16]. In PERSIANN-CDR, the IR data are firstly applied in the PERSIANN model to produce historical rainfall estimates, then these estimates are bias adjusted by using the Global Precipitation Climatology Project 2.5° monthly data [16]. Currently, the available PERSIANN-CDR is daily temporal resolution and 0.25° spatial resolution for the 60° S–60° N latitude band.

2.2.2. Gauged Precipitation and Discharge Data

Daily precipitation data for the year of 2000–2013 were obtained from 22 rain gauge stations in Xixian Basin (Figure 1). The same long-term series daily streamflow and meteorological data were obtained from the Xixian hydrologic station and Xinyang evaporation station, respectively. The Penman–Monteith equation was used to calculate daily potential evapotranspiration as one forcing input data for the hydrological model [35]. The inverse distance weighting method was used to interpolate the rain gauge data into the spatial distribution [36]. The 30 arc-second global digital elevation model data was collected from the U.S. Geological Survey [37]. The vegetation-type data were collected from the Moderate Resolution Imaging Spectroradiometer land cover data using the International Geosphere–Biosphere Program classification system [38].

3. Methodology

3.1. Evaluation Statistics

In the present study, three statistical indices were adopted to qualitatively evaluate the precision of the six SPPs. The Person correlation coefficient (CC) assesses the correlation between satellite precipitation products and rain gauge observations. The root-mean-square error (RMSE) measures the average error magnitude of satellite precipitation. In addition, the relative bias (BIAS) demonstrates the systematic bias of satellite precipitation. Two categorical statistical indices, named probability of detection (POD) and false-alarm rate (FAR), represent the correspondence between SPPs and rain gauge data [39]. POD, also named hit rate, shows how often rain occurrences are correctly detected by satellite. FAR denotes the fraction of cases in which satellite records precipitation when rain gauge does not. A precipitation threshold of 1.0 mm was used to define rain or no-rain events in this study. The CC, BIAS, and Nash–Sutcliffe coefficient (NSE) comprehensively reflect the hydrologic model performance on the basis of the observed and simulated streamflow [40]. Formulas to calculate the indices mentioned above are listed in Table 1.

Table 1. Statistical evaluation indices for evaluating the SPPs and their hydrological utility.

Evaluation Indices	Unit	Formulas	Perfect Value
Correlation coefficient (CC)	NA	$CC = \frac{\sum_{i=1}^n (G_i - \bar{G})(S_i - \bar{S})}{\sqrt{\sum_{i=1}^n (G_i - \bar{G})^2} \sqrt{\sum_{i=1}^n (S_i - \bar{S})^2}}$	1
Root-mean-square error (RMSE)	mm	$RMSE = \sqrt{\frac{1}{n} \sum_{i=1}^n (S_i - G_i)^2}$	0
Relative bias (BIAS)	%	$BIAS = \frac{\sum_{i=1}^n (S_i - G_i)}{\sum_{i=1}^n G_i} \times 100\%$	0
Probability of detection (POD)	NA	$POD = \frac{t_H}{t_H + t_M}$	1
False-alarm rate (FAR)	NA	$FAR = \frac{t_F}{t_H + t_F}$	0
Nash–Sutcliffe coefficient (NSE)	NA	$NSCE = 1 - \frac{\sum_{i=1}^n (Q_{sim}(i) - Q_{obs}(i))^2}{\sum_{i=1}^n (Q_{obs}(i) - \bar{Q}_{obs})^2}$	1

Notes: where n is the total amount of samples; S_i and G_i are the i th values of the evaluated data and reference data, respectively; \bar{S} and \bar{G} are the mean values of the S_i and G_i , respectively. H , M , and F are different cases: H , observed rain correctly detected; M , observed rain not detected; F , rain detected but not observed. t_H , t_M , and t_F are the times of occurrence of the corresponding case. The details of these parameters can be found in Ebert et al. [39].

3.2. Hydrological Model and Calibration

Xinanjiang model (XAJ model) is a famous physically-based conceptual rainfall-runoff model developed by Zhao [41]. It has been widely used in different humid river basins over China [42,43]. In the current study, a grid-based XAJ model was constructed. The model calculated the total runoff within each grid unit using the saturation excess runoff scheme. The total runoff was divided into surface runoff, soil runoff and underground runoff using an overflow reservoir with bottom and side holes. Then the linear reservoir was used to perform the slope runoff convergence and the Muskingum segmentation flood routing was used to perform the river network runoff convergence. The model contains 15 parameters (see Table 2), and they were automatically calibrated through the Shuffled Complex Evolution (SCE-UA) global optimization algorithm proposed by Duan et al. [44]. In the current study, the XAJ model was calibrated with rain gauge precipitation data at daily time scale and $0.25^\circ \times 0.25^\circ$ spatial resolution. In addition, the model runs were then repeated with the six SPPs as inputs. We determined the January 2000 to December 2006 as calibration period and January 2007 to December 2013 as validation period.

Table 2. Parameters of the XAJ model and their prior ranges.

Parameter	Physical Meaning	Prior Range
Kc	ratio of potential evapotranspiration to pan evaporation	0.5–1.5
WUM	water capacity in the upper soil layer	10–40
WLM	water capacity in the lower soil layer	50–90
WDM	water capacity in the deeper soil layer	10–70
B	exponent of tension water capacity curve	0.1–0.5
C	coefficient of deep evapotranspiration	0.1–0.3
EX	exponent of free water capacity curve	1–1.5
SM	free water capacity of surface soil layer	10–60
KI0	outflow coefficients of free water storage to interflow	KI + KG = 0.7
KG0	outflow coefficients of free water storage to groundwater	0.1–0.5
CI0	recession constant of the lower interflow storage	0.1–0.9
CG0	daily recession constant of groundwater storage	0.9–0.999
CS0	recession constant for channel routing	0.1–0.5
KE	slot storage coefficient	20–24
XE	flow proportion factor	0.1–0.5

4. Results and Discussion

4.1. Evaluation of Satellite Precipitation Products

The selected six SPPs covering the entire Xixian Basin from 1 January 2000 to 31 December 2013 (in which TMPA 3B42RT and PERSIANN-RT were from 1 March 2000) were evaluated in terms of errors in daily precipitation, extreme precipitation, and monthly precipitation.

4.1.1. Daily Precipitation Evaluation

Scatterplots of the basin average daily precipitation estimates of six SPPs versus rain gauge observations are shown in Figure 2, and the statistical measures of six SPPs for the daily scale are summarized in Table 3. Among the three real-time SPPs, CMORPH-RT exhibits the best performance with the highest CC of 0.79 and CSI of 0.55 and lowest RMSE of 5.42 mm, BIAS of -12.60 , and FAR of 0.26. TMPA 3B42RT presents a performance comparable to that of CMORPH-RT, except for a large overestimation of precipitation estimates, with BIAS of 23.75%. The performance of PERSIANN-RT is the worst among those of the three real-time SPPs. For the three post-real-time research SPPs, TMPA 3B42V7 and CMORPH-CRT present better performance than that of the latest PERSIANN-CDR. As documented in many prior studies, the two post-real-time research SPPs of TMPA and CMORPH exhibit much better performance than that of their corresponding real-time satellite precipitation [18,21]. With regard to PERSIANN products, the newly released post-real-time research version PERSIANN-CDR insignificantly improves precipitation estimates compared with the real-time PERSIANN-RT does at daily time scale. Therefore, caution should be exercised when applying the newly released PERSIANN-CDR for daily quantitative precipitation estimation at similar river basins. In general, TMPA and CMORPH (especially the two post-real-time research SPPs) show good performance for daily precipitation estimates over Xixian Basin.

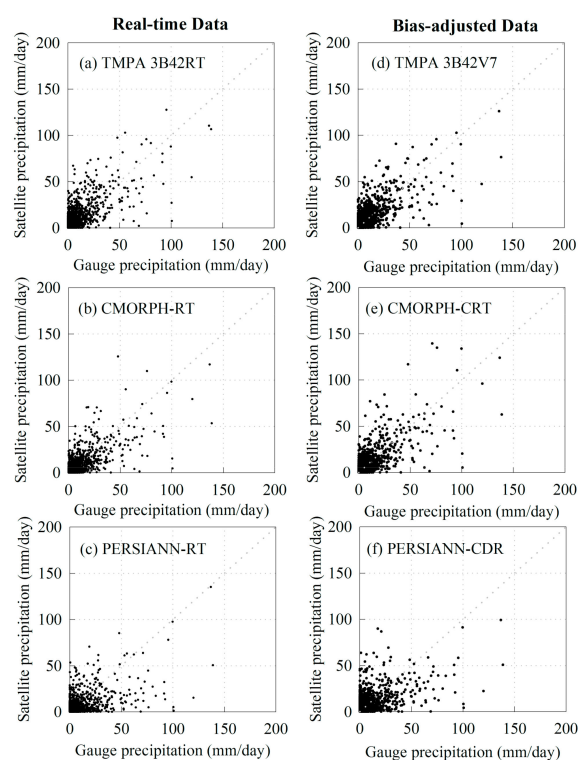


Figure 2. Scatterplots of the basin average daily precipitation between SPPs and rain gauge observations for Xixian Basin: (a) TMPA 3B42RT; (b) CMORPH-RT; (c) PERSIANN-RT; (d) TMPA 3B42V7; (e) CMORPH-CRT; (f) PERSIANN-CDR.

Table 3. Statistical measures of the SPPs for the daily precipitation estimates.

Products	CC	RMSE (mm)	BIAS (%)	POD	FAR
TMPA 3B42RT	0.76	6.17	25.25	0.75	0.36
CMORPH-RT	0.76	5.65	−11.87	0.67	0.28
PERSIANN-RT	0.59	7.06	−17.20	0.62	0.47
TMPA 3B42V7	0.78	5.71	15.10	0.76	0.30
CMORPH-CRT	0.77	5.84	9.20	0.73	0.31
PERSIANN-CDR	0.60	7.15	19.04	0.76	0.56

4.1.2. Extreme Precipitation Evaluation

Three extreme precipitation indices, namely, annual maximum 1-day precipitation ($R \times 1$ d), 3-day precipitation ($R \times 3$ d), and 5-day precipitation ($R \times 5$ d) [27], were adopted to evaluate the performance of the six SPPs in capturing the behavior of precipitation extremes. The statistical measures of the SPPs for $R \times 1$ d, $R \times 3$ d, and $R \times 5$ d are summarized in Table 4, and the box plots of the BIAS values of $R \times 1$ d, $R \times 3$ d, and $R \times 5$ d of the six SPPs are shown in Figure 3. Among the three real-time SPPs, TMPA 3B42RT exhibits the best performance in capturing the behavior of precipitation extremes with comparable CC and the lowest RMSE, and BIAS, whereas TMPA 3B42RT still shows serious overestimation of $R \times 1$ d, $R \times 3$ d, and $R \times 5$ d for some years (Figure 3). Notably, the BIAS values of the three near-real-time products, as shown in the box plots of Figure 3, are distributed in a wider range than that of their corresponding post-real-time products. This result indicates the great uncertainty of the near-real-time SPPs in capturing the behavior of precipitation extremes. For the three post-real-time research SPPs, TMPA 3B42V7 and CMORPH-CRT present much better performance than that of the latest PERSIANN-CDR which seriously underestimates precipitation extremes precipitation extremes. With regard to the multiple indicators, TMPA 3B42V7 and CMORPH-CRT exhibit good performance in capturing the behavior of precipitation extremes over Xixian Basin, whereas they still present certain underestimations of precipitation extremes. This finding is consistent with that of a few previous works [18,32]. Other time consistency uncertainties are observed in the performance of SPPs in capturing precipitation extremes. Table 5 shows the occurrence date of $R \times 1$ d detection by rain gauge observations and six SPPs for the period of 2000–2013. Among the six SPPs, TMPA 3B42RT and CMORPH-RT show the best performance in time consistency for detecting the occurrence date of $R \times 1$ d. The two SPPs are followed by TMPA 3B42V7 and CMORPH-CRT. The PERSIANN products exhibit the worst performance. In general, most occurrence dates of $R \times 1$ d detection by SPPs are still inconsistent with the date detected by gauge observations. Thus, owing to the underestimation in precipitation extremes and the inconsistency of occurrence time with rain gauge observations, caution should be exercised when applying the current TMPA, CMORPH, and PERSIANN products in predicting extreme precipitation at such medium-sized humid basin.

Table 4. Statistical measures of the SPPs for annual maximum 1-, 3-, and 5-day precipitation.

Extreme Precipitation Indices	Products	CC	RMSE (mm)	BIAS (%)
$R \times 1$ d	TMPA 3B42RT	0.74	22.05	−5.90
	CMORPH-RT	0.73	26.06	−15.36
	PERSIANN-RT	0.76	29.34	−23.70
	TMPA 3B42V7	0.88	19.99	−14.54
	CMORPH-CRT	0.84	18.99	−3.64
	PERSIANN-CDR	0.74	34.21	−30.29
$R \times 3$ d	TMPA 3B42RT	0.67	44.76	4.82
	CMORPH-RT	0.71	46.06	−16.55
	PERSIANN-RT	0.67	59.76	−31.52
	TMPA 3B42V7	0.87	30.41	−8.92
	CMORPH-CRT	0.79	35.55	−1.42
	PERSIANN-CDR	0.87	49.89	−27.91
$R \times 5$ d	TMPA 3B42RT	0.71	47.31	4.91
	CMORPH-RT	0.75	50.87	−20.35
	PERSIANN-RT	0.56	67.00	−28.52
	TMPA 3B42V7	0.88	31.24	−7.27
	CMORPH-CRT	0.85	34.11	−7.53
	PERSIANN-CDR	0.78	47.95	−18.27

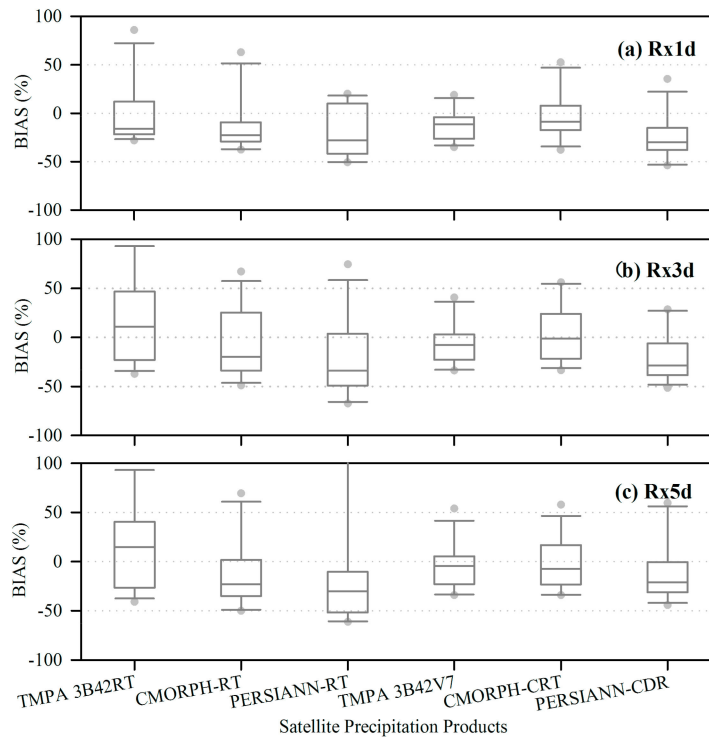


Figure 3. Box plots of the BIAS index of the annual maximum (a) 1-day precipitation; (b) 3-day precipitation and (c) 5-day precipitation for the six SPPs versus rain gauge observations over 14 years. The upper and lower edges of the box mark the upper and lower quartiles (75% and 25%, respectively); the solid line in the box marks the median value; the upper and lower horizontal lines out of the box mark the 90% and 10% quartiles, respectively; the points mark the maximum and minimum values.

Table 5. Occurrence date of annual maximum 1-day precipitation ($R \times 1$ d) detection by rain gauge observations and six SPPs for the period of 2000–2013. Gray boxes indicate the date of $R \times 1$ d detected by SPPs is consistent with the date detected by rain gauge observations.

Year	Gauge	TM PA 3B42RT	CMORPH-RT	PERSIANN-RT	TM PA 3B42V7	CMORPH-CRT	PERSIANN-CDR
2000	8/18	6/1	6/1	6/1	6/1	6/1	6/1
2001	6/17	7/29	8/7	7/21	10/25	10/25	7/26
2002	6/22						
2003	6/29	7/20	4/17	4/17	10/10	8/24	8/28
2004	8/4						7/16
2005	7/9		6/25	6/25	6/25	8/28	6/25
2006	9/4	6/29	5/4	7/21	5/4	5/4	7/21
2007	7/13	5/30	5/30	5/30	7/8	7/8	7/4
2008	7/22	8/13	8/13	7/17	8/13	8/13	7/17
2009	8/28	6/27	6/27	7/21	5/27	8/17	5/27
2010	7/16			5/3			9/6
2011	7/26						6/13
2012	9/7	8/26		7/7	8/26	8/26	8/18
2013	8/22						

4.1.3. Monthly Precipitation Evaluation

The daily precipitation estimates from the six SPPs were aggregated to monthly time series and were then compared with the rain gauge-observed monthly precipitation. Figure 4 depicts the scatterplots of the basin average monthly precipitation from SPPs and rain gauge observations. Similar to the daily results, among the three real-time SPPs, CMORPH-RT presents the best performance with the highest CC of 0.91 and the lowest RMSE of 39.78 mm, and BIAS of -12.60% . TMPA 3B42RT exhibits

a performance comparable to that of CMORPH-RT except for a large overestimation of precipitation estimates. PERSIANN-RT takes the last place because of the lowest CC of 0.82 and the largest RMSE of 57.51 mm. For the three post-real-time research SPPs, TMPA 3B42V7 and CMORPH-CRT show much better performance than that of the newly released PERSIANN-CDR. At monthly time scale, all three post-real-time research products of TMPA 3B42V7, CMORPH-CRT, and PERSIANN-CDR outperform their corresponding real-time estimates (Figure 4), suggesting that the monthly time scale gauge adjustments applied to the TMPA, CMORPH, and PERSIANN systems substantially improve the monthly data accuracy of retrievals. The month-to-month gauge-adjusted post-real-time research products are suggested as ideal SPPs for monthly water resource condition analysis.

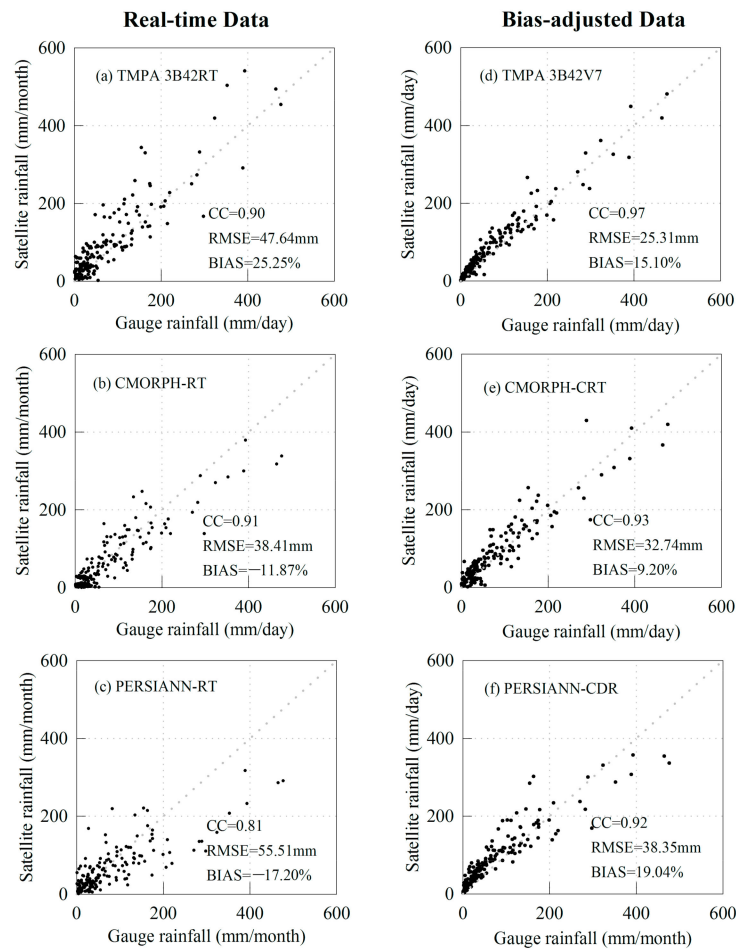


Figure 4. Scatterplots of the basin average monthly precipitation between SPPs and rain gauge observations for Xixian Basin: (a) TMPA 3B42RT; (b) CMORPH-RT; (c) PERSIANN-RT; (d) TMPA 3B42V7; (e) CMORPH-CRT; (f) PERSIANN-CDR.

4.2. Evaluation of Streamflow Simulations

The streamflow simulation accuracy when the model was calibrated on the basis of rain gauge data was analyzed to evaluate the streamflow simulation utility of the six SPPs. The simulated streamflow using the six SPPs as inputs were compared with the observed streamflow in the following three aspects.

4.2.1. Daily Streamflow Evaluation

Figure 5a compares the rain gauge data-simulated daily hydrograph with that observed streamflow and summarizes the statistical measures of the rain gauge data-simulated results. There are

good agreements between the observed and simulated daily streamflow series. The statistical indices, with daily CC of 0.92 and 0.90, NSE of 0.85 and 0.81, and BIAS of -2.54% and 9.71% for the calibration and validation periods, respectively, demonstrate that the XAJ model can have good simulations of the streamflow.

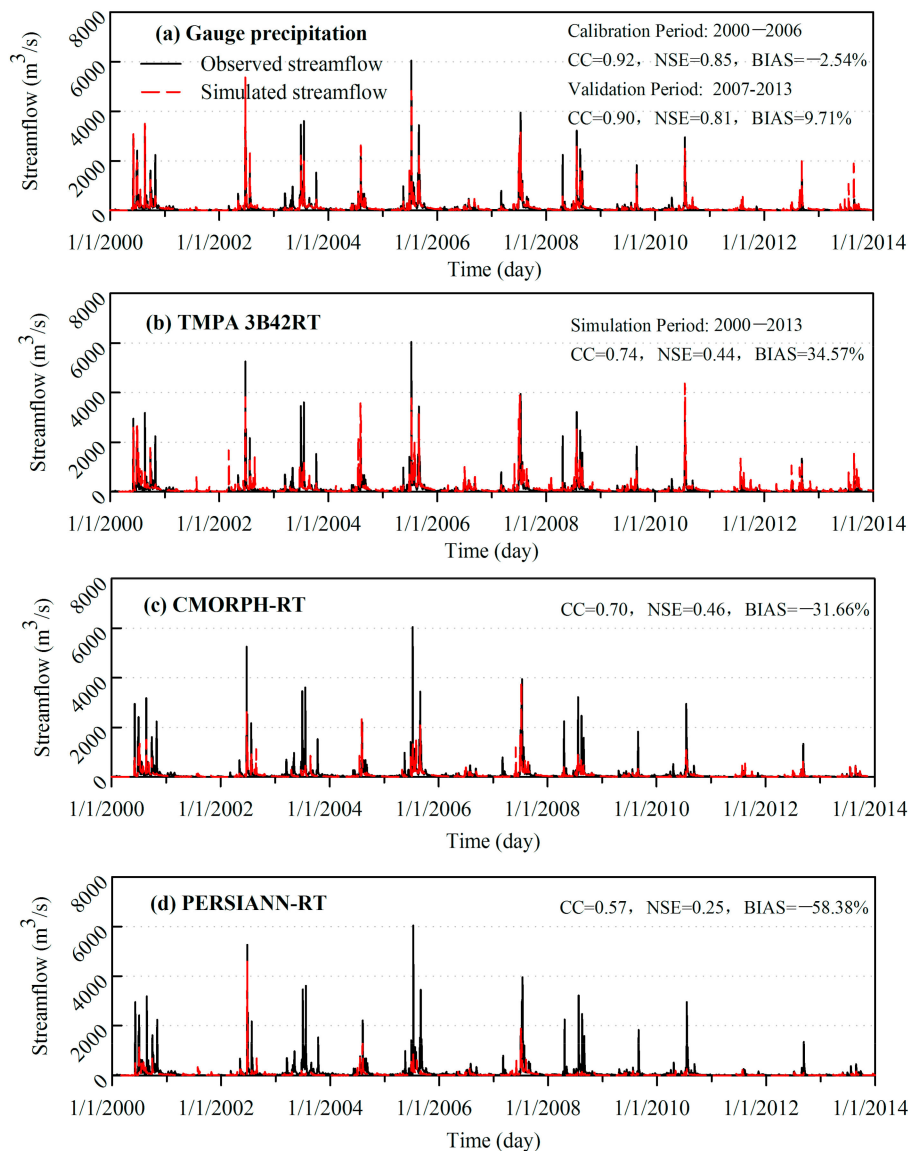


Figure 5. Observed and XAJ model-simulated daily streamflows from the rain gauge observations and the three real-time SPPs for (a) rain gauge precipitation; (b) TMPA 3B42RT; (c) CMORPH-RT and (d) PERSIANN-RT.

The calibrated XAJ model was then forced by the six SPPs as inputs in the period of 2000–2013. Figure 5b–d show the XAJ model-simulated daily streamflows from the three real-time SPPs, and Figure 6a–c depicts the XAJ model-simulated daily streamflows from the three post-real-time research SPPs. For the three real-time SPPs, the simulations of TMPA 3B42RT have significant overestimation of most streamflow series for its systematic overestimation of precipitation. On the contrary, the simulations of CMORPH-RT and PERSIANN-RT significant underestimation of most streamflow series for their systematic underestimation of precipitation. The streamflow simulation of TMPA 3B42RT presents daily CC of 0.74, daily NSE of 0.44, and BIAS of 32.68% for the entire simulation period. The streamflow simulation of CMORPH-RT exhibits daily CC of 0.70, daily NSE of 0.46,

and BIAS of -29.90% for the entire simulation period. The streamflow simulation of PERSIANN-RT shows daily CC of 0.57, daily NSE of 0.26, and BIAS of -54.41% for the entire simulation period. Generally, the three near-real-time SPPs produce much worse hydrologic predictions with increased error propagation from input to streamflow at daily time scale, which implies the necessity of bias adjustment or uncertainty analysis for the three near-real-time SPPs in hydrological application [45].

The simulations of the three post-real-time research products clearly outperform those from their corresponding real-time estimates. The streamflow simulation of TMPA 3B42V7, which presents daily CC of 0.80, daily NSE of 0.62, and BIAS of 15.07% for the entire simulation period, fits best with the observed streamflow series among those of the six SPPs (Figures 5 and 6). This SPP-based simulation is followed by the CMORPH-CRT-based simulation, which exhibits daily CC of 0.73, daily NSE of 0.51, and BIAS of 3.26% . The simulation from PERSIANN-CDR performs worse, with daily CC of 0.63, daily NSE of 0.39, and BIAS of -10.22% . However, all the SPP-based streamflow simulations observably underestimate a few high peak flows in the rainy seasons. This result is mainly attributed to the precipitation estimate uncertainty of SPPs at the daily time scale and the model parameterization uncertainties when calibrated it on the basis of rain gauge data [17,45].

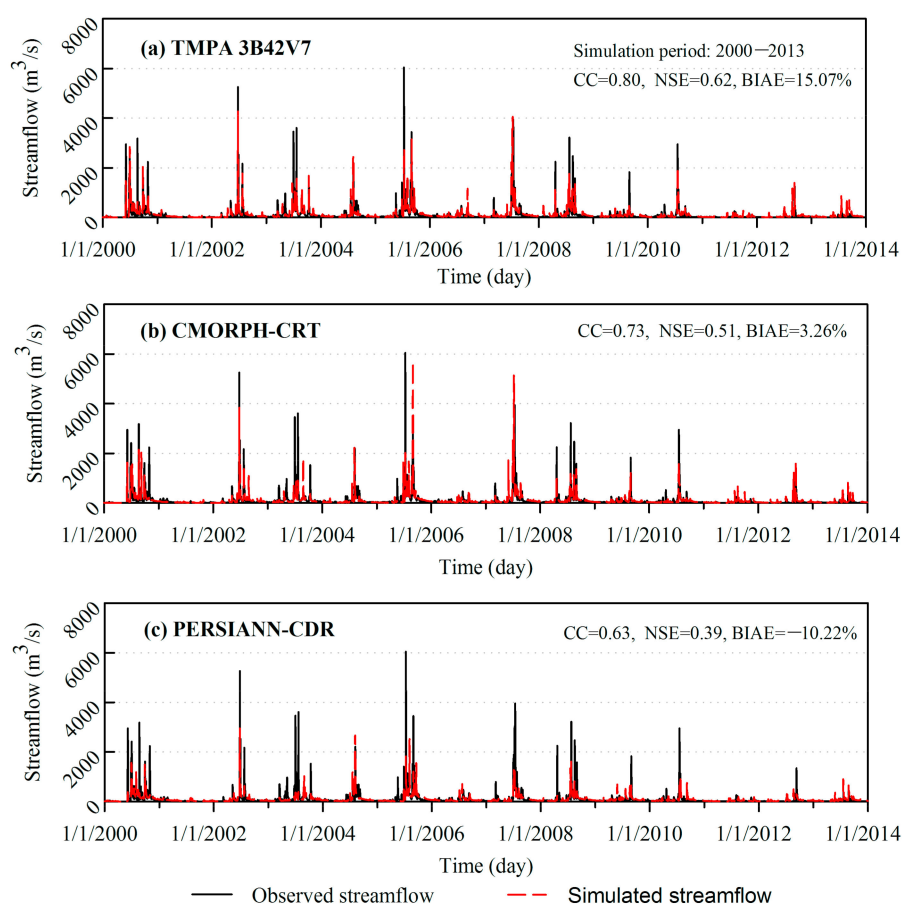


Figure 6. Observed and XAJ model-simulated daily streamflows from the three bias-adjusted SPPs for (a) TMPA 3B42V7; (b) CMORPH-CRT and (c) PERSIANN-CDR.

4.2.2. Extreme Streamflow Evaluation

Three extreme streamflow indices, namely, annual maximum 1-day streamflow ($Q \times 1$ d), 3-day streamflow ($Q \times 3$ d), and 5-day streamflow ($Q \times 5$ d) [18], were adopted to evaluate the performance of the six SPPs in simulating streamflow extremes. Table 6 provides the statistical measures of the SPPs-simulated $Q \times 1$ d, $Q \times 3$ d, and $Q \times 5$ d. Figure 7 shows the box plots of the BIAS index of $Q \times 1$

d, $Q \times 3$ d, and $Q \times 5$ d for the SPP-based simulations versus hydrological gauge observations. Among the six SPPs, the $Q \times 1$ d, $Q \times 3$ d, and $Q \times 5$ d simulated from CMORPH-RT, PERSIANN-RT, and PERSIANN-CDR seriously underestimate the observed extreme streamflow. The TMPA 3B42RT-based simulation exhibits the smallest BIAS values but presents wider range of distribution of the BIAS box plot than its corresponding post-real-time product, indicating the great uncertainty in TMPA 3B42RT-simulated streamflow extremes (Figure 7). TMPA 3B42V7 and CMORPH-CRT present good performance in simulating $Q \times 1$ d, $Q \times 3$ d, and $Q \times 5$ d, with acceptable CC, RMSE, and BIAS values compared with those of the rain gauge simulations (Table 6). For further analysis of the time consistency uncertainty of the SPPs in simulating streamflow extremes, Table 7 shows the occurrence date of $Q \times 1$ d simulated by gauge observations and six SPPs for the period of 2000–2013. Compared with the extreme precipitation analysis results, the consistencies in the occurrence dates of $Q \times 1$ d simulated by SPPs improved (Tables 5 and 7). The $Q \times 1$ d simulated by TMPA 3B42RT and CMORPH-RT are consistent for 9 and 8 years with the $Q \times 1$ d observed by hydrological station during the 14 years. This finding is comparable to the rain gauge data-simulated results. The consistencies in occurrence dates of $Q \times 1$ d for TMPA 3B42V7 and CMORPH-CRT, which are 6 and 7 years, respectively, are slightly worse than those of their corresponding real-time data. The PERSIANN products show the worst consistencies in occurrence dates compared with TMPA and CMORPH products. Although the near-real-time TMPA and CMORPH products present acceptable consistencies in occurrence dates of $Q \times 1$ d, their simulation biases are non-ignorable. In general, the month-to-month gauge-adjusted TMPA 3B42V7 and CMORPH-CRT exhibit good utility in simulating streamflow extremes, although they still show non-ignorable deviation and occurrence time inconsistency problems compared with gauge-based results. Thus, uncertainties should be considered when applying the current TMPA, CMORPH, and PERSIANN products in simulating extreme streamflow at such medium-sized humid basin.

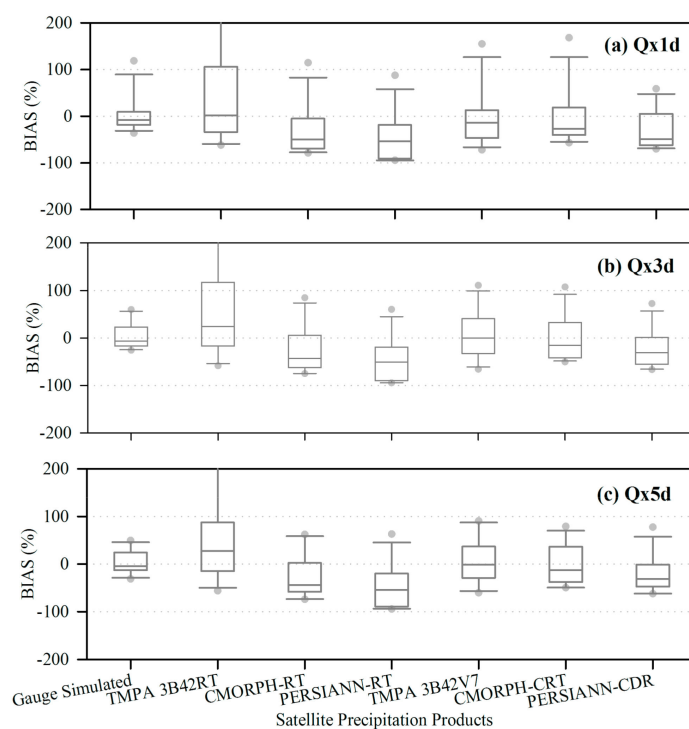


Figure 7. Box plots of the BIAS index of the annual maximum (a) 1-day streamflow; (b) 3-day streamflow and (c) 5-day streamflow for the six SPPs-based simulations versus the hydrological station observations over 14 years.

Table 6. Statistical measures of the SPPs simulated annual maximum 1-, 3-, and 5-day streamflow.

Extreme Streamflow Indices	Products	CC	RMSE (m ³ /s)	BIAS (%)
Q × 1 d	Gauge Simulation	0.95	622.24	−9.36
	TMPA 3B42RT	0.72	1271.30	−6.87
	CMORPH-RT	0.68	1880.36	−48.23
	PERSIANN-RT	0.55	2337.10	−64.04
	TMPA 3B42V7	0.84	1219.34	−24.92
	CMORPH-CRT	0.87	1034.61	−18.83
	PERSIANN-CDR	0.78	1828.34	−48.75
Q × 3 d	Gauge Simulation	0.94	1245.83	1.72
	TMPA 3B42RT	0.68	2874.90	13.22
	CMORPH-RT	0.61	3539.83	−39.75
	PERSIANN-RT	0.48	4574.23	−57.37
	TMPA 3B42V7	0.78	2259.33	−10.01
	CMORPH-CRT	0.82	2336.19	−6.98
	PERSIANN-CDR	0.69	3241.86	−37.03
Q × 5 d	Gauge Simulation	0.95	1455.22	3.54
	TMPA 3B42RT	0.69	3636.28	17.25
	CMORPH-RT	0.64	4233.58	−38.22
	PERSIANN-RT	0.50	5581.75	−56.42
	TMPA 3B42V7	0.79	2719.15	−5.50
	CMORPH-CRT	0.79	3017.57	−7.34
	PERSIANN-CDR	0.70	3814.52	−33.47

Table 7. Occurrence date of annual maximum 1-day streamflow (Q × 1 d) simulated by rain gauge observations and six SPPs for the period of 2000–2013. Gray boxes indicate the date of Q × 1 d simulated by each precipitation product is consistent with the date detected by gauge observations.

Year	Observation	Gauge	TMPA 3B42RT	CMORPH-RT	PERSIANN-RT	TMPA 3B42V7	CMORPH-CRT	PERSIANN-CDR
2000	8/20		6/30		6/29	6/30		6/27
2001	2/1	7/26	7/31	8/1	7/28	1/28	10/27	2/2
2002	6/24							
2003	7/22	7/1		8/26	6/23	10/12	8/26	8/30
2004	8/6							
2005	7/11			8/30		8/30	8/30	8/4
2006	7/30	9/6	7/2	7/2	7/23	9/10	9/10	7/23
2007	7/15		7/9	7/10	7/4	7/10	7/10	7/10
2008	7/24				7/19		8/31	7/24
2009	8/30				7/23			5/29
2010	7/19							7/26
2011	8/4	8/11	7/28	8/18	7/28	10/3	8/18	8/18
2012	9/10				7/9			8/22
2013	8/26					7/21		7/21

4.2.3. Monthly Runoff Evaluation

Figure 8 shows the observed and XAJ model-simulated monthly runoffs from the six SPPs. The statistical measures of the SPP-simulated runoffs were calculated for the period of 2000–2013. Similar to the daily results, for the three real-time SPPs, the simulations of TMPA 3B42RT significantly overestimate most of the streamflow series, whereas the simulations of CMORPH-RT and PERSIANN-RT significantly underestimate most of the runoff series. The simulations of the three post-real-time research products obviously outperform those from their corresponding real-time estimates. The simulation from TMPA 3B42V7 shows monthly CC of 0.93, monthly NSE of 0.86, and BIAS of 15.07% for the period of 2000–2013. The simulation from CMORPH-CRT presents monthly CC of 0.88, monthly NSE of 0.78, and BIAS of 3.26%. The simulation from PERSIANN-CDR shows monthly CC of 0.81, monthly NSE of 0.62, and BIAS of −10.22%. In general, the three month-to-month gauge-adjusted post-real-time research products can simulate acceptable monthly runoff series over Xixian Basin.

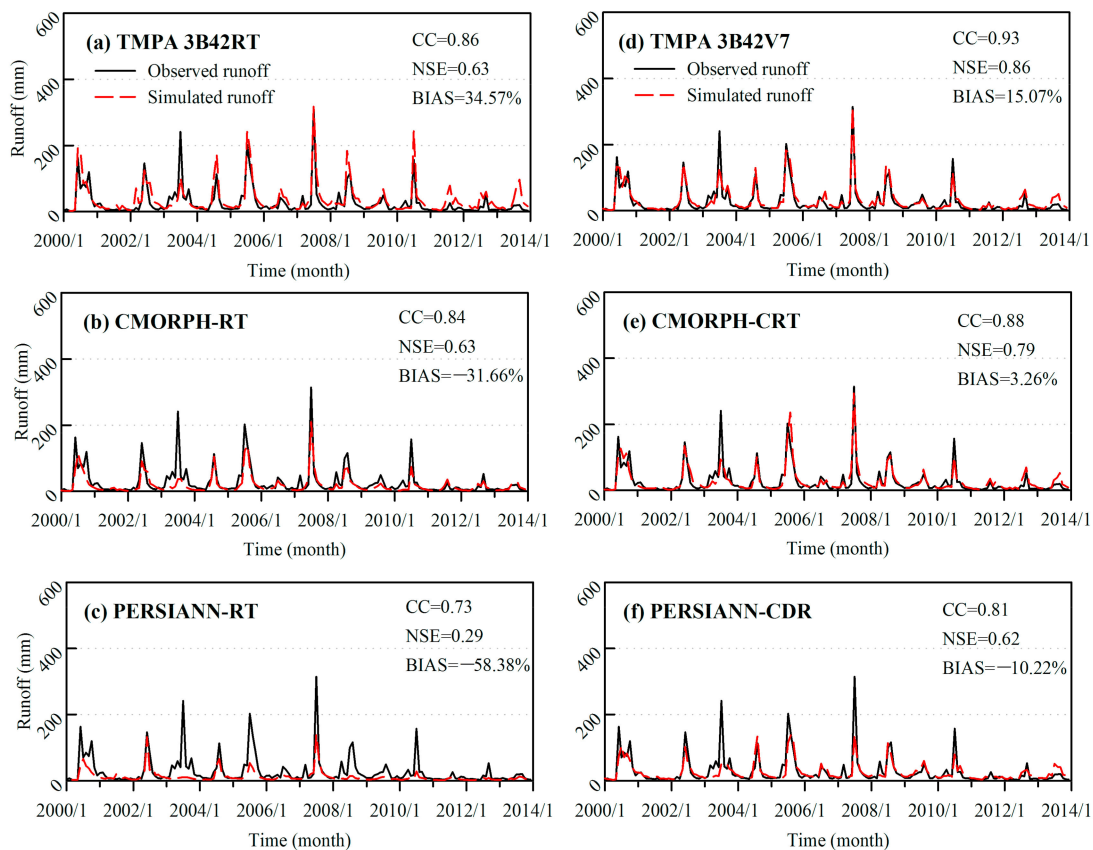


Figure 8. Observed and XAJ model-simulated monthly runoffs from the six SPPs for (a) TMPA 3B42RT; (b) CMORPH-RT; (c) PERSIANN-RT; (d) TMPA 3B42V7; (e) CMORPH-CRT and (f) PERSIANN-CDR. The statistical measures of the SPPs-simulated streamflows were calculated for the period of 2000–2013.

5. Conclusions

This study evaluated the hydrological performance of six mainstream SPPs (i.e., TMPA 3B42RT, CMORPH-RT, PERSIANN-RT, TMPA 3B42V7, CMORPH-CRT, and PERSIANN-CDR) via direct comparison of rain gauge observations and hydrological model streamflow simulations over a medium-sized humid basin in central eastern China. The evaluation specifically focused on the performance of the six SPPs in capturing extreme precipitation and extreme streamflow. The conclusions were summarized as follows.

Among the three real-time SPPs, the CMORPH-RT exhibits the best performance, while the TMPA 3B42RT and PERSIANN-RT reveal non-ignorable system errors. The bias adjustment or uncertainty analysis are suggested for practical application of the current real-time SPPs. The two post-real-time research products of TMPA 3B42V7 and CMORPH-CRT exhibit much better performance than that of their corresponding real-time SPPs for daily precipitation estimation. By contrast, the newly released post-real-time research product PERSIANN-CDR insignificantly improves daily precipitation estimate compared with the real-time PERSIANN-RT does. Caution should be exercised when applying the newly released PERSIANN-CDR for daily quantitative precipitation estimation at similar river basins. Moreover, all three post-real-time research products of TMPA 3B42V7, CMORPH-CRT, and PERSIANN-CDR obviously outperform those of real-time estimates at monthly time scale. The month-to-month gauge-adjusted post-real-time research products are suggested as ideal SPPs for monthly water resource condition analysis.

The daily streamflow simulations of the three post-real-time research products clearly outperform those from their corresponding real-time estimates. The streamflow simulation of TMPA 3B42V7

fits best with the observed streamflow series among those of the six SPPs. In general, all six SPP-based streamflow simulations observably underestimate a few high peak flows in the rainy seasons. This finding is mainly attributed to the SPP data uncertainty at the daily time scale and the model parameterization uncertainties when calibrated it on the basis of rain gauge data. Meanwhile, the three month-to-month gauge-adjusted post-real-time research products can simulate acceptable monthly runoff series. This result shows that the three post-real-time research products present good application potentiality in monthly water resources monitoring and management.

For extreme precipitation detection, TMPA 3B42V7 and CMORPH-CRT exhibit much better performance than those of other SPPs in capturing the behavior of precipitation extremes over Xixian Basin, but they still underestimate the precipitation extremes. Most occurrence dates of $R \times 1$ d detection by SPPs are inconsistent with the date detection by gauge observations. For extreme streamflow simulation, TMPA 3B42V7 and CMORPH-CRT present good performance, although they still show non-ignorable deviation and occurrence time inconsistency problems compared with rain gauge observed results. Caution should be exercised when applying the current TMPA, CMORPH, and PERSIANN products for monitoring and predicting extreme precipitation and flood at such medium-sized basin.

Acknowledgments: This work was financially supported by the National Key Research and Development Program approved by Ministry of Science and Technology, China (2016YFA0601504); the National Natural Science Foundation of China (41501017, 51779070); the Fundamental Research Funds for the Central Universities (2017B10214); the Natural Science Foundation of Jiangsu Province (BK20150815); and the Programme of Introducing Talents of Discipline to Universities by the Ministry of Education and the State Administration of Foreign Experts Affairs, China (B08048).

Author Contributions: Shanhu Jiang and Liliang Ren designed the framework of this study; Linqi Zhang, Menghao Wang and Yujie Lu collected and processed the data; Shanhu Jiang and Shuya Liu analyzed the data and wrote the paper; Bin Yong and Yingqing He provided significant suggestions on the methodology and structure of the manuscript.

Conflicts of Interest: The authors declare no conflict of interest.

References

1. Blöschl, G.; Hall, J.L.; Parajka, J.; Perdigao, R.A.P.; Merz, B.; Arheimer, B.; Aronica, G.T.; Bilibashi, A.; Bonacci, Q.; Borga, M.; et al. Changing climate shifts timing of European floods. *Science* **2017**, *357*, 588–590. [[CrossRef](#)] [[PubMed](#)]
2. Desai, B.; Maskrey, A.; Peduzzi, P.; De Bono, A.; Herold, C. *Making Development Sustainable: The Future of Disaster Risk Management, Global Assessment Report on Disaster Risk Reduction*; United Nations Office for Disaster Risk Reduction (UNISDR): Genève, Suisse, 2015.
3. Hong, Y.; Adler, R.F.; Hossain, F.; Curtis, S.; Huffman, G.J. A first approach to global runoff simulation using satellite rainfall estimation. *Water Resour. Res.* **2007**, *43*. [[CrossRef](#)]
4. Yu, M.Y.; Chen, X.; Li, L.H.; Bao, A.M.; Paix, M.J. Streamflow Simulation by SWAT Using Different Precipitation Sources in Large Arid Basins with Scarce Rain gauges. *Water Resour. Manag.* **2011**, *25*, 2669–2681. [[CrossRef](#)]
5. Jiang, S.H.; Ren, L.L.; Hong, Y.; Yong, B.; Yang, X.L.; Yuan, F.; Ma, M.W. Comprehensive Evaluation of Multi-satellite Precipitation Products with a Dense Rain Gauge Network and Optimally Merging their Simulated Hydrological Flows using the Bayesian Model Averaging Method. *J. Hydrol.* **2012**, *452–453*, 213–225. [[CrossRef](#)]
6. Wu, H.; Adler, R.F.; Tian, Y.D.; Huffman, G.J.; Li, H.Y.; Wang, J.J. Real-time global flood estimation using satellite-based precipitation and a coupled land surface and routing model. *Water Resour. Res.* **2014**, *50*. [[CrossRef](#)]
7. Kidd, C.; Huffman, G. Global precipitation measurement. *Meteorol. Appl.* **2011**, *18*, 334–353. [[CrossRef](#)]
8. Yong, B.; Liu, D.; Gourley, J.J.; Tian, Y.D.; Huffman, G.J.; Ren, L.L.; Hong, Y. Global View of Real-Time Trmm Multisatellite Precipitation Analysis: Implications for Its Successor Global Precipitation Measurement Mission. *Bull. Am. Meteorol. Soc.* **2015**, *96*, 283–296. [[CrossRef](#)]

9. Wang, Z.L.; Zhong, R.D.; Lai, C.G.; Chen, J.C. Evaluation of the GPM IMERG satellite-based precipitation products and the hydrological utility. *Atmos. Res.* **2017**, *196*, 151–163. [[CrossRef](#)]
10. Sorooshian, S.; Hsu, K.L.; Gao, X.G.; Gupta, H.V.; Imam, B.; Braithwaite, D. Evaluation of PERSIANN system satellite-based estimates of tropical rainfall. *Bull. Am. Meteorol. Soc.* **2000**, *81*, 2035–2046. [[CrossRef](#)]
11. Joyce, R.J.; Janowiak, J.E.; Arkin, P.A.; Xie, P.P. CMORPH: A method that produces global precipitation estimates from passive microwave and infrared data at high spatial and temporal resolution. *J. Hydrometeorol.* **2004**, *5*, 487–503. [[CrossRef](#)]
12. Huffman, G.J.; Adler, R.F.; Bolvin, D.T.; Gu, G.J.; Nelkin, J.; Bowman, K.P.; Hong, Y.; Stocker, F.; Wolff, D.B. The TRMM Multisatellite Precipitation Analysis (TMPA): Quasi-Global, multiyear, combined-sensor precipitation estimates at fine scales. *J. Hydrometeorol.* **2007**, *8*, 38–55. [[CrossRef](#)]
13. Hou, A.Y.; Kakar, R.K.; Neeck, S.; Azarbarzin, A.A.; Kummerow, C.D.; Kojima, M.; Oki, R.; Nakamura, K.; Iguchi, T. The Global Precipitation Measurement Mission. *Bull. Am. Meteorol. Soc.* **2014**, *95*, 701–722. [[CrossRef](#)]
14. Huffman, G.J.; Bolvin, D.T. *Real-Time TRMM Multi-Satellite Precipitation Analysis Data Set Documentation*; National Aeronautics and Space Administration: Washington, DC, USA, 2013.
15. Xie, P.P.; Joyce, R.; Wu, S.R.; Yoo, S.H.; Yarosh, Y.; Sun, F.; Lin, R. Reprocessed, Bias-Corrected CMORPH Global High-Resolution Precipitation Estimates from 1998. *J. Hydrometeorol.* **2017**, *18*, 1617–1641. [[CrossRef](#)]
16. Ashouri, H.; Hsu, K.L.; Sorooshian, S.; Braithwaite, D.K.; Knapp, K.R.; Cecil, D.; Nelson, B.R.; Prat, O.P. PERSIANN-CDR: Daily Precipitation Climate Data Record from Multisatellite Observations for Hydrological and Climate Studies. *Bull. Am. Meteorol. Soc.* **2015**, *96*, 69–83. [[CrossRef](#)]
17. Yong, B.; Chen, B.; Gourley, J.J.; Ren, L.L.; Hong, Y.; Chen, X.; Wang, W.G.; Chen, S.; Gong, L.Y. Intercomparison of the Version-6 and Version-7 TMPA precipitation products over high and low latitudes basins with independent gauge networks: Is the newer version better in both real-time and post-real-time analysis for water resources and hydrologic extremes? *J. Hydrol.* **2014**, *508*, 77–87.
18. Zhu, Q.; Xuan, W.D.; Liu, L.; Xu, Y.P. Evaluation and hydrological application of precipitation estimates derived from PERSIANN-CDR, TRMM 3B42V7, and NCEP-CFSR over humid regions in China. *Hydrol. Process.* **2016**, *30*, 3061–3083. [[CrossRef](#)]
19. Ashouri, H.; Nguyen, P.; Thorstensen, A.; Hsu, K.L.; Sorooshian, S.; Braithwaite, D. Assessing the Efficacy of High-Resolution Satellite-Based PERSIANN-CDR Precipitation Product in Simulating Streamflow. *J. Hydrometeorol.* **2016**, *17*, 2061–2076. [[CrossRef](#)]
20. Duan, Z.; Liu, J.Z.; Tuo, Y.; Chiogna, G.; Disse, M. Evaluation of eight high spatial resolution gridded precipitation products in Adige Basin (Italy) at multiple temporal and spatial scales. *Sci. Total Environ.* **2016**, *573*, 1536–1553. [[CrossRef](#)] [[PubMed](#)]
21. Jiang, S.H.; Ren, L.L.; Yong, B.; Hong, Y.; Yang, X.L.; Yuan, F. Evaluation of Latest TMPA and CMORPH Precipitation Products with Independent Rain Gauge Observation Networks over High-latitude and Low-latitude Basins in China. *Chin. Geogr. Sci.* **2016**, *26*, 439–455. [[CrossRef](#)]
22. Hussain, Y.; Satge, F.; Hussain, M.B.; Martinez-Carvajal, H.; Bonnet, M.P.; Cardenas-Soto, M.; Roig, H.L.; Akhter, G. Performance of CMORPH, TMPA, and PERSIANN rainfall datasets over plain, mountainous, and glacial regions of Pakistan. *Theor. Appl. Climatol.* **2017**. [[CrossRef](#)]
23. Alazzy, A.A.; Lu, H.S.; Chen, R.S.; Ali, A.B.; Zhu, Y.H.; Su, J.B. Evaluation of Satellite Precipitation Products and Their Potential Influence on Hydrological Modeling over the Ganzi River Basin of the Tibetan Plateau. *Adv. Meteorol.* **2017**. [[CrossRef](#)]
24. Yuan, F.; Zhang, L.M.; Win, K.W.W.; Ren, L.L.; Zhao, C.X.; Zhu, Y.H.; Jiang, S.H.; Liu, Y. Assessment of GPM and TRMM Multi-Satellite Precipitation Products in Streamflow Simulations in a Data-Sparse Mountainous Watershed in Myanmar. *Remote Sens.* **2017**, *9*, 302. [[CrossRef](#)]
25. Gourley, J.J.; Hong, Y.; Flamig, Z.L.; Wang, J.H.; Vergara, H.; Anagnostou, E.N. Hydrologic Evaluation of Rainfall Estimates from Radar, Satellite, Gauge, and Combinations on Ft. Cobb Basin, Oklahoma. *J. Hydrometeorol.* **2011**, *12*, 973–988. [[CrossRef](#)]
26. Huang, Y.; Chen, S.; Cao, Q.; Hong, Y.; Wu, B.W.; Huang, M.Y.; Qiao, L.; Zhang, Z.X.; Li, Z.; Yang, X.Q. Evaluation of Version-7 TRMM Multi-Satellite Precipitation Analysis Product during the Beijing Extreme Heavy Rainfall Event of 21 July 2012. *Water* **2014**, *6*, 32–44. [[CrossRef](#)]

27. Miao, C.Y.; Ashouri, H.; Hsu, K.-L.; Sorooshian, S.; Duan, Q.Y. Evaluation of the PERSIANN-CDR daily rainfall estimates in capturing the behavior of extreme precipitation events over China. *J. Hydrometeorol.* **2015**, *16*, 1387–1396. [[CrossRef](#)]
28. Zhang, Y.; Hong, Y.; Wang, X.G.; Gourley, J.J.; Xue, X.W.; Saharia, M.; Ni, G.H.; Wang, G.L.; Huang, Y.; Chen, S.; et al. Hydrometeorological Analysis and Remote Sensing of Extremes: Was the July 2012 Beijing Flood Event Detectable and Predictable by Global Satellite Observing and Global Weather Modeling Systems? *J. Hydrometeorol.* **2015**, *16*, 381–395. [[CrossRef](#)]
29. Shah, H.L.; Mishra, V. Uncertainty and Bias in Satellite-Based Precipitation Estimates over Indian Subcontinental Basins: Implications for Real-Time Streamflow Simulation and Flood Prediction. *J. Hydrometeorol.* **2016**, *17*, 615–636. [[CrossRef](#)]
30. Bharti, V.; Singh, C.; Ettema, J.; Turkington, T.A.R. Spatiotemporal characteristics of extreme rainfall events over the Northwest Himalaya using satellite data. *Int. J. Climatol.* **2016**, *36*, 3949–3962. [[CrossRef](#)]
31. Mei, Y.W.; Nikolopoulos, E.I.; Anagnostou, E.N.; Zoccatelli, D.; Borga, M. Error Analysis of Satellite Precipitation-Driven Modeling of Flood Events in Complex Alpine Terrain. *Remote Sens.* **2016**, *8*, 293. [[CrossRef](#)]
32. Jiang, S.S.; Zhang, Z.X.; Huang, Y.H.; Chen, X.; Chen, S. Evaluating the TRMM Multisatellite Precipitation Analysis for Extreme Precipitation and Streamflow in Ganjiang River Basin, China. *Adv. Meteorol.* **2017**, *2017*. [[CrossRef](#)]
33. Wang, R.; Chen, J.Y.; Wang, X.W. Comparison of IMERG Level-3 and TMPA 3B42V7 in Estimating Typhoon-Related Heavy Rain. *Water* **2017**, *9*, 276. [[CrossRef](#)]
34. Yang, Y.M.; Du, J.; Cheng, L.L.; Xu, W. Applicability of TRMM satellite precipitation in driving hydrological model for identifying flood events: A case study in the Xiangjiang River Basin, China. *Nat. Hazards* **2017**, *87*, 1489–1505. [[CrossRef](#)]
35. Allen, R.G.; Pereira, L.S.; Raes, D.; Smith, M. *Crop Evapotranspiration—Guidelines for Computing Crop Water Requirements—FAO Irrigation and Drainage Paper 56*; United Nations Food and Agriculture Organization: Rome, Italy, 1998.
36. Bartier, P.M.; Keller, C.P. Multivariate interpolation to incorporate thematic surface data using Inverse Distance Weighting (IDW). *Comput. Geosci.* **1996**, *22*, 795–799. [[CrossRef](#)]
37. Global 30 Arc-Second Elevation (GTOPO30). Available online: <https://lta.cr.usgs.gov/GTOPO30> (accessed on 28 December 2017).
38. Friedl, M.A.; McIver, D.K.; Hodges, J.C.F.; Zhang, X.Y.; Muchoney, D.; Strahler, A.H.; Woodcock, C.E.; Gopal, S.; Schneider, A.; Cooper, A.; et al. Global land cover mapping from MODIS: Algorithms and early results. *Remote Sens. Environ.* **2002**, *83*, 287–302. [[CrossRef](#)]
39. Ebert, E.E.; Janowiak, J.E.; Kidd, C. Comparison of near-real-time precipitation estimates from satellite observations and numerical models. *Bull. Am. Meteorol. Soc.* **2007**, *88*, 47–64. [[CrossRef](#)]
40. Nash, J.E.; Sutcliffe, J.V. River flow forecasting through conceptual models, Part 1: A discussion of principles. *J. Hydrol.* **1970**, *10*, 282–290. [[CrossRef](#)]
41. Zhao, R.J. The Xinanjiang model applied in China. *J. Hydrol.* **1992**, *135*, 371–381.
42. Xu, H.L.; Xu, C.Y.; Chen, S.D.; Chen, H. Similarity and difference of global reanalysis datasets (WFD and APHRODITE) in driving lumped and distributed hydrological models in a humid region of China. *J. Hydrol.* **2016**, *542*, 343–356. [[CrossRef](#)]
43. Jiang, S.H.; Ren, L.L.; Xu, C.Y.; Liu, S.Y.; Yuan, F.; Yang, X.L. Quantifying multi-source uncertainties in multi-model predictions using the Bayesian model averaging scheme. *Hydrol. Res.* **2017**. [[CrossRef](#)]
44. Duan, Q.Y.; Sorooshian, S.; Gupta, V.K. Optimal use of the SCE-UA global optimization method for calibrating watershed models. *J. Hydrol.* **1994**, *158*, 265–284. [[CrossRef](#)]
45. Jiang, S.H.; Ren, L.L.; Hong, Y.; Yang, X.L.; Ma, M.W.; Zhang, Y.; Yuan, F. Improvement of Multi-Satellite Real-Time Precipitation Products for Ensemble Streamflow Simulation in a Middle Latitude Basin in South China. *Water Resour. Manag.* **2014**, *28*, 2259–2278. [[CrossRef](#)]

